SERCA-mediated calcium uptake in the DBA/2J vs C57BL/10 mdx models of Duchenne muscular dystrophy

Riley EG Cleverdon[1,2], Kennedy C Whitley[1,2], Daniel M Marko[3], Sophie I Hamstra[1,2], Jessica L Braun[1,2], Brian D Roy[1,2], Rebecca EK MacPherson[3,4], Val A Fajardo[1,2,4]*

[1] Department of Kinesiology, Brock University, St. Catharines, Ontario, Canada.
[2] Centre for Bone and Muscle Health, Brock University, St. Catharines, Ontario, Canada.
[3] Department of Health Sciences, Brock University, St. Catharines, ON L2S 3A1, Canada.
[4] Centre for Neuroscience, Brock University, St. Catharines, ON L2S 3A1, Canada.

The authors have declared that no conflict of interest exists.

Corresponding author:
Val A. Fajardo, PhD
Assistant Professor
Department of Kinesiology
Brock University
1812 Sir Isaac Brock Way
L2S 3A1
vfajardo@brocku.ca

Abstract

The C57BL/10ScSn-*Dmd*^{mdx}/J (C57 *mdx*) mouse is the most commonly used murine model of Duchenne muscular dystrophy (DMD) but displays a mild phenotype with a late onset, greatly limiting translatability to clinical research. In consequence, the D2.B10-*Dmd*^{mdx}/J (D2 *mdx*) mouse was created and produces a more severe, early onset phenotype. Mechanistic insights of the D2 *mdx* phenotype have yet to be elucidated, specifically related to sarcoplasmic reticulum (SR) calcium (Ca^{2+}) handling. In our study, we aimed to determine if SR Ca^{2+} handling differences in the D2 *mdx* versus the C57 *mdx* mouse could explain model phenotypes. Firstly, analyses determined that D2 *mdx* mice ambulate less and have weaker muscles, but have greater energy expenditure than C57 counterparts. SR Ca^{2+} handling measures determined that only D2 *mdx* mice have impaired SR calcium intake in the gastrocnemius, left ventricle and diaphragm. This was coupled with decrements in maximal sarco-endoplasmic reticulum Ca^{2+}-ATPase (SERCA) activity and greater activation of the Ca^{2+}-activated protease, calpain, in the gastrocnemius. Overall, our study is the first to determine that SR Ca^{2+} handling is impaired in the D2 *mdx* mouse, specifically at the level of the SERCA pump.

44 **Introduction**

45 Duchenne muscular dystrophy (DMD) is an X-linked recessive muscle wasting disease,
46 affecting approximately 1 in 3,500 boys worldwide (1, 2). Symptoms of DMD typically begin at
47 three or four years of age and with no cure to date, patients usually succumb to cardiorespiratory
48 complications from the disease by the third or fourth decade of life (3–5). Caused by the complete
49 loss of dystrophin, a protein that normally connects the cytoskeleton and extracellular matrix to
50 the sarcolemma, DMD is characterized by excessive membrane tearing and myofibre
51 damage/degeneration (6). Loss of dystrophin is the initial insult of DMD, however there are several
52 secondary consequences of the disease including chronic inflammation, oxidative stress, and
53 calcium (Ca^{2+}) overload (7). Combined, these processes ultimately lead to the pathological
54 hallmarks of DMD which include degeneration, necrosis, and fatty and fibrotic replacement of
55 muscular tissue (8).

56 Ca^{2+} is a potent signaling molecule largely responsible for excitation-contraction coupling
57 (ECC) in skeletal and cardiac muscle. Two major Ca^{2+} regulatory proteins involved in muscle ECC
58 are the ryanodine receptor (RyR) and sarco-endoplasmic reticulum ATPase (SERCA) pump,
59 located in the sarcoplasmic reticulum (SR). RyR is responsible for the release of Ca^{2+} from the SR
60 into the myoplasm, which initiates cross-bridge formation and force generation, whereas SERCA
61 catalyzes the reuptake of Ca^{2+} into the SR to initiate muscle relaxation (9, 10). However, several
62 studies have shown that if SR Ca^{2+} handling is dysregulated, Ca^{2+} can become chronically elevated
63 in the myoplasm, leading to muscle damage and weakness. Indeed, impaired Ca^{2+} handling is a
64 major part of the pathology in the muscles of patients living with DMD. The resulting Ca^{2+}
65 overload exacerbates oxidative stress, inflammation, and cellular necrosis which in turn
66 perpetuates dystrophic pathology (11, 12). Further, RyR and SERCA function are implicated in

67 dystrophic muscles. For example, RyR leak has been shown to occur in excessive amounts caused
68 by both depletion of the channel stabilizer calstabin and elevated reactive oxygen and nitrogen
69 species (RONS) modifications to RyR1 (13). SERCA has also been shown to have impaired
70 maximal Ca^{2+} uptake in murine models of DMD (14). Like RyR1, SERCA dysfunction in
71 dystrophic muscles can also be partly attributed to RONS stress leading to damaging protein
72 modifications (15).

73 The C57BL/10ScSn-*Dmd*^{mdx}/J (C57 *mdx*) mouse, originally discovered in 1984, has served
74 as the dominant *in vivo* model to study cellular mechanisms and potential therapies for DMD (16).
75 However, with a mild dystrophic pathology that is slow to progress, researchers have sought out
76 alternative models that may better recapitulate human DMD (17). For example, previous research
77 has shown that SERCA pump function is more severely impaired in the *mdx*/utrophin double
78 knockout mouse – a severe DMD mouse model where both dystrophin and its functional homolog
79 utrophin are completely absent (14). While this suggests that Ca^{2+} dysregulation may also partly
80 contribute to the worsened pathology and weakness observed in the double knockout mouse
81 model, it is important to note that this model does not genotypically represent DMD. More
82 recently, the traditional C57 *mdx* mouse was backcrossed onto a DBA/2J background, giving way
83 to the D2.B10-*Dmd*^{mdx}/J (D2 *mdx*) mouse (18). Unlike the C57 *mdx* mouse, the D2 *mdx* mouse
84 presents with a juvenile onset and more severe DMD pathology, including pronounced muscle
85 weakness and damage, degeneration, fibrosis, necrosis, and inflammation (18–20). The underlying
86 mechanisms behind the greater pathology displayed in D2 *mdx* mice compared to C57 *mdx* mice
87 are still under investigation, though a recent report has implicated elevated TGF- β signalling (21).
88 However, to our knowledge SR Ca^{2+} handling has yet to be characterized in the D2 *mdx* mouse.
89 Therefore, we examined SR Ca^{2+} handling in 8-10-week-old D2 and C57 *mdx* mice. This cohort

was selected based on previous studies showing that D2 *mdx* mice at this age display muscle weakness and pathology whereas the C57 *mdx* mice do not (18–20). We hypothesized that severity in pathology related to weakness observed in D2 *mdx* mice compared to the C57 *mdx* mice would be associated with greater impairments to SR Ca^{2+} handling.

Results

Muscle weakness and wasting in the C57 mdx versus D2 mdx mice

We first sought to verify the phenotypical weakness and atrophy previously reported in the D2 *mdx* mice. As expected, serum CK was elevated in both *mdx* strains with a significant main effect of *mdx* genotype (Figure 1A). Moreover, gastrocnemius muscle and body mass were significantly lower in the D2 strain, with a significant interaction with *mdx* genotype indicating that body mass was lower in *mdx* vs WT mice, however only for the D2 *mdx* mouse (Figure 1B and C). When normalized to body mass, a significant main effect of strain was found suggesting that the gastrocnemius:body mass ratio was lower in D2 mice compare with C57 (Figure 1D). Holding impulse, or hangwire time normalized to body mass, was significantly lower across both *mdx* strains (Figure 1E). However, planned comparisons indicate that D2 *mdx* mice have less holding impulse compared with C57 *mdx* mice ($p < 0.05$, Student's t-test), consistent with previous reports of muscle weakness in the D2 *mdx* mice (Figure 1F).

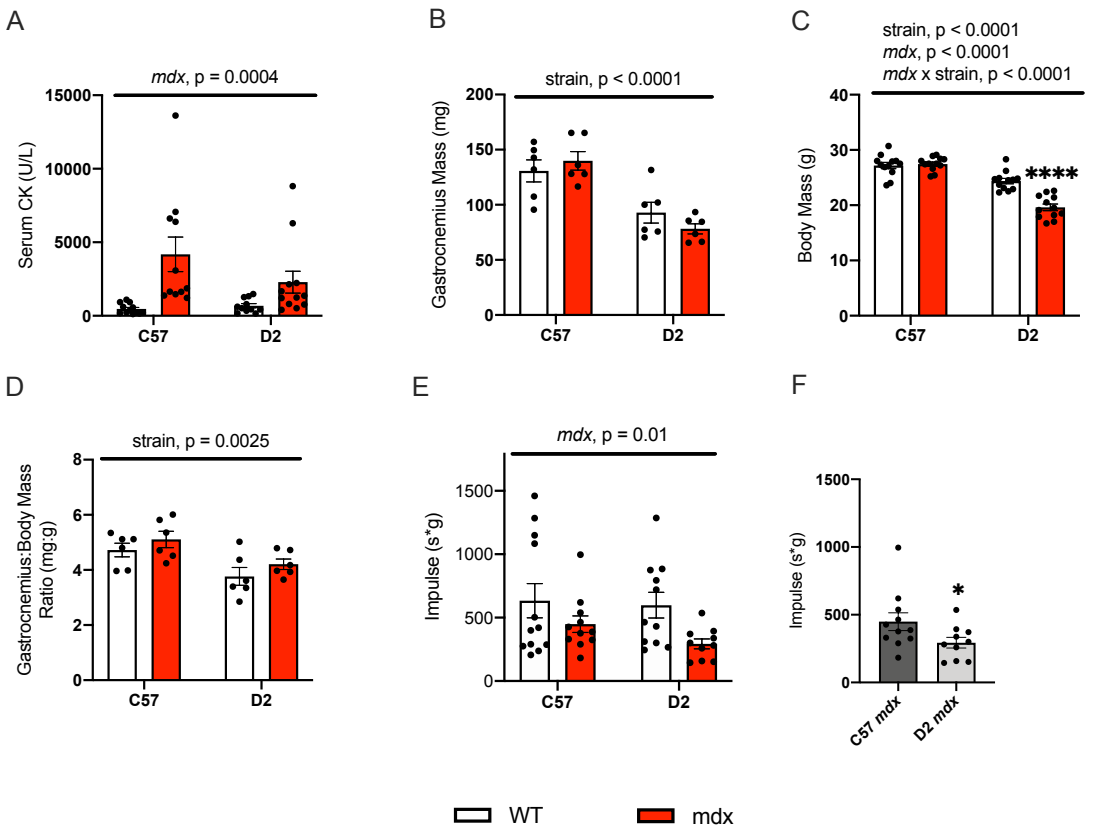

Figure 1: Creatine kinase, muscle/body mass and impulse: A) Serum creatine kinase activity expressed in units per litre. B) Gastrocnemius mass (mg), C) body mass (g), and D) gastrocnemius mass:body mass ratio (mg:g). E) Impulse expressed as hangwire time*body mass. F) Planned comparison of impulse. A two-way ANOVA or Students' t-test was used for all comparisons, n=12 per group. Values are represented as mean ± SEM. Main effects and interactions expressed in bars over the graph, ****$p < 0.0001$ using a Sidak's post-hoc test.

142 *Metabolic phenotyping of the C57 mdx and D2 mdx mice*

143 In further support of the apparent muscle weakness in the D2 *mdx* mice, metabolic cage
144 data indicate that only the D2 *mdx* mice and not the C57 *mdx* mice were less ambulant in their
145 cages (Figure 2A and B). We also found that the D2 *mdx* mice and not the C57 *mdx* mice had
146 elevated daily energy expenditure compared to WT (Figure 2C and D), with significant and
147 trending reductions in food and water intake, respectively (Figure 2E-H). The Promethion
148 metabolic cage system also allows for certain behavioural analyses including time spent in or
149 touching its 'home' – a habitat enclosure on a slightly elevated platform. In both cases, we found
150 that the D2 *mdx* mice spent less time in the habitat and interacting with the habitat compared to
151 D2 WT mice, whereas these differences were not observed in the C57 *mdx* and C57 WT mice
152 (Figure 2 I-L). We believe that this serves as an additional indication of muscle weakness, whereby
153 the D2-*mdx* mice were not strong enough to enter the elevated enclosure.

154

155

156

157

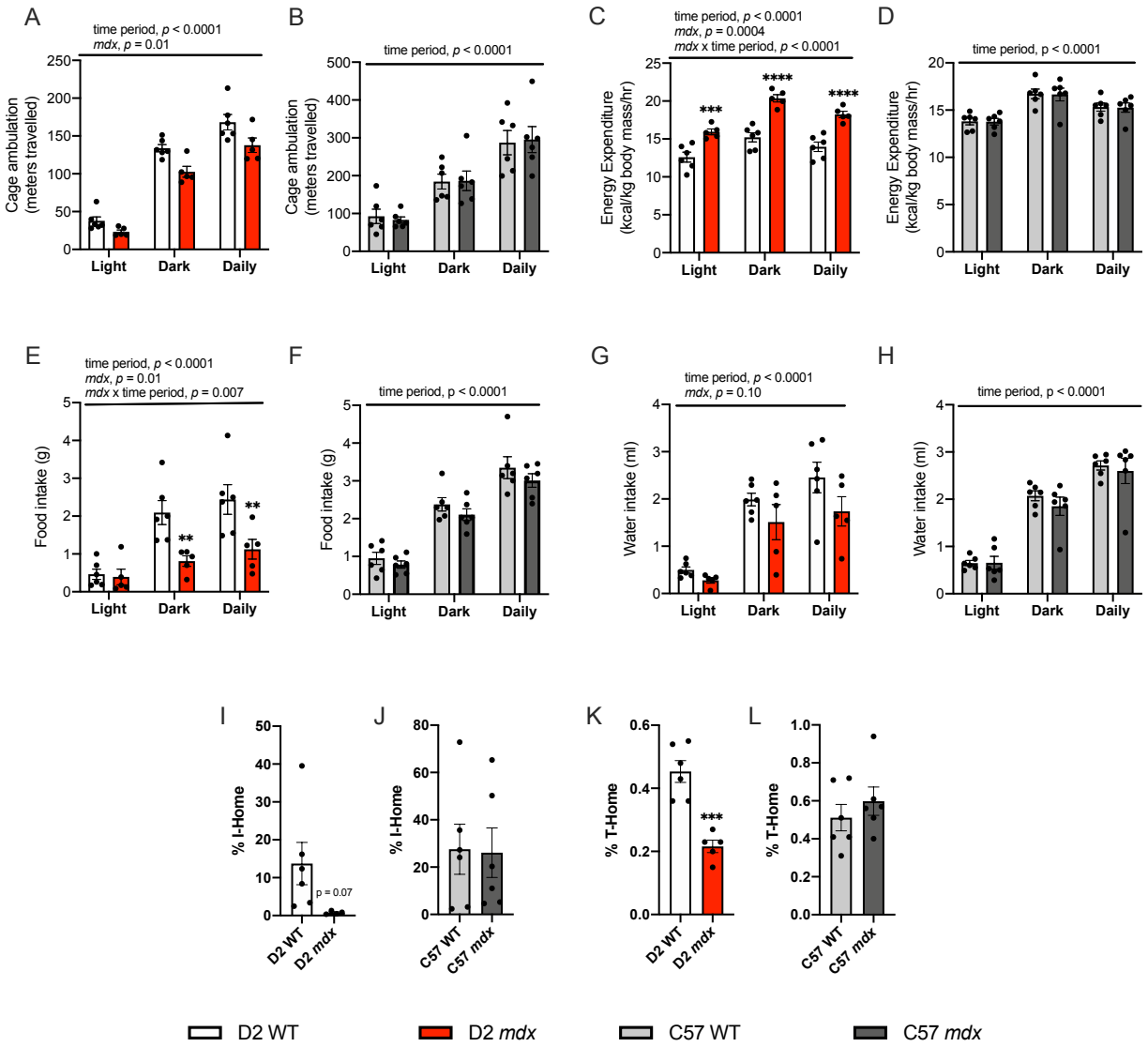

Figure 2. Cage activity, energy expenditure and cage behaviour: A) Daily cage ambulation in D2 mice and B) C57 mice expressed in metres travelled. C) Energy expenditure in D2 mice and D) C57 mice expressed in kcal/kg of body mass/hr. E) and G) Food (g) and water (mL) intake of D2 mice and F) and H) C57 mice. Percentage of time spent in (I-Home) and interacting with (T-Home) the mouse home for D2 mice I) and K) and C57 mice J) and L). All metabolic cage analyses were measured over a 48-hour period. Two-way repeated ANOVA examining the effect of time period, *mdx* genotype and their potential interaction (A-H). $^{**}p < 0.01$, $^{***}p < 0.001$, and $^{****}p < 0.0001$ using a Sidak's post-hoc test, n = 5-6 per group. Student's t-test examined WT versus mdx (I-L), n = 5-6 per group. Values are represented as mean ± SEM.

172 *SR Ca^{2+} uptake/filling and SERCA activity is impaired in D2 mdx mice but not C57 mdx mice*

173 We then examined SR Ca^{2+} handling in gastrocnemius muscles from C57 and D2 -WT and
174 -*mdx* mice (Figure 3). SR Ca^{2+} uptake experiments revealed impairments in the D2 *mdx* mice
175 compared with WT mice but not C57 *mdx* mice (Figure 3A). A significant main effect of *mdx*
176 genotype was found with starting $[Ca^{2+}]_{free}$ likely reflective of the Ca^{2+} overload present in the *mdx*
177 muscles. However, a significant interaction revealed that only the D2 *mdx* muscles had elevated
178 starting $[Ca^{2+}]_{free}$ compared with D2 WT as this was not observed in the C57 strain (Figure 3B).
179 Similarly, AUC calculated from the Ca^{2+} uptake curves revealed a significant main effect of *mdx*
180 genotype with AUC being higher in the *mdx* mice. However, a significant interaction indicated
181 that this was only statistically significant for D2 WT vs D2 *mdx* and not C57 WT vs C57 *mdx*
182 (Figure 3C). In addition, while maximum rates of Ca^{2+} uptake did not differ from C57 WT, C57
183 *mdx* and D2 WT mice we were unable to obtain a viable rate for D2 *mdx* mice (Figure 3D). When
184 CPA was added to induce Ca^{2+} leak, D2 *mdx* mice had the least amount of leak from the SR, likely
185 reflective of impaired SR Ca^{2+} filling during the uptake period (Figure 3E and F). We then
186 measured Ca^{2+}-dependent SERCA ATPase activity in the gastrocnemius muscle (Figure 3G and
187 H). We found a trending interaction ($p = 0.058$) between *mdx* and strain indicating that maximal
188 SERCA activity was impaired in gastrocnemius muscles from D2 *mdx* mice compared with D2
189 WT, but this was not observed in the C57 *mdx* and WT mice (Figure 3I). No changes in SERCA's
190 apparent affinity for Ca^{2+} (pCa_{50}) were found (Figure 3J). Nevertheless, our Ca^{2+} uptake and
191 SERCA activity findings demonstrated defective SR Ca^{2+} handling only in the D2 *mdx* mice. To
192 determine a potential pathological consequence of Ca^{2+} dysregulation calpain activity was
193 measured in the gastrocnemius. We found that calpain activity was higher in the *mdx* strains
194 compared with their respective WTs, and that D2 mice generally had greater calpain activity

195 compared to C57 mice (Figure 3K). Furthermore, planned comparisons between D2 *mdx* and C57
196 *mdx* showed that calpain activity was significantly higher in D2 *mdx* mice ($p = 0.0006$, Student's
197 t-test).
198
199
200
201
202

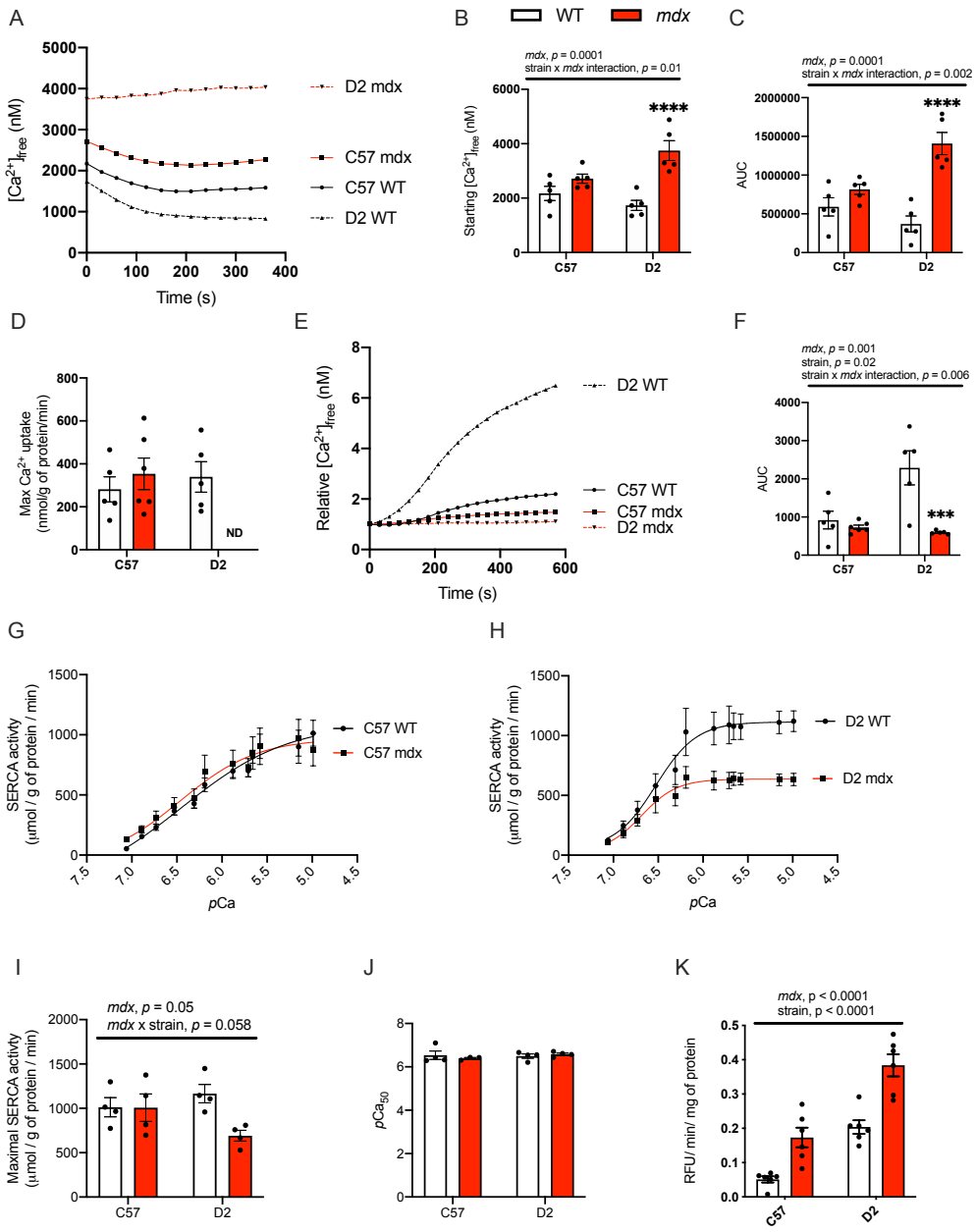

Figure 3: SR Ca^{2+} uptake/leak, SERCA and calpain activity in C57 and D2 -WT and -*mdx* gastrocnemius muscle: A) Ca^{2+} uptake curves from gastrocnemius homogenates. B) Starting $[Ca^{2+}]_{free}$ levels immediately after ATP addition. C) Area under the curve (AUC) of Ca^{2+} uptake curves. D) Maximum rate of Ca^{2+} uptake obtained from the Ca^{2+} uptake curves expressed as nmol/g of protein/min. E) Ca^{2+} leak curve after the addition of cyclopiazonic acid (CPA) and expressed relative to baseline Ca^{2+} immediately after CPA addition. The addition of CPA inhibits the SERCA pump allowing for SR Ca^{2+} to be released back into the cytosol. F) AUC analysis of SR Ca^{2+} leak. G) & H) Ca^{2+}-dependent SERCA activity curves in D2 and C57 -WT and -*mdx* gastrocnemius muscles. I) Maximal SERCA activity expressed as µmol/g of protein/min and J) pCa_{50} of SERCA activity, n = 4. K) Calpain activity in gastrocnemius muscles from D2 and C57 -WT and -*mdx* gastrocnemius muscles expressed as RFU min/mg of protein. Two-way ANOVAs were performed with a Sidak's post-hoc test, $*p < 0.05$, $**p < 0.01$, $***p < 0.001$, and $****p < 0.0001$ n= 5-6. Main effects and interactions expressed in bars over the graph. Values are represented as mean ± SEM.

216 *Elevated RONS may contribute to impaired SR filling*

217 To examine the potential mechanisms explaining the defective SR Ca^{2+} handling in D2
218 *mdx* mice, we performed western blotting of SR Ca^{2+} handling proteins (Figure 4). Our results
219 showed that SERCA1a content was upregulated in both *mdx* strains (Figure 4A). SERCA2a
220 content was upregulated in the *mdx* strains, however, a significant interaction indicated that this
221 was only in the D2 *mdx* mice (Figure 4B). Sarcolipin (SLN) is a known inhibitor of SERCA that
222 is upregulated in *mdx* mice (22) and was ectopically expressed in both the D2 *mdx* and C57 *mdx*
223 gastrocnemius muscle; however, C57 *mdx* mice had a significantly higher content compared with
224 D2 *mdx* (Figure 4C). RyR1 content was also altered with a significant main effect of strain showing
225 lower RyR1 in D2 mice compared with C57 mice; and a significant main effect of *mdx* genotype
226 showing reduced RyR1 content in *mdx* mice (Figure 4D). Calstabin, the channel stabilizer of RyR1
227 did not have any significant changes in protein content (Figure 4E), however, when expressed as
228 a ratio to RyR1, D2 *mdx* mice had significantly higher levels of calstabin relative to RyR1 (Figure
229 4F). We also investigated protein nitrosylation and nitration in the gastrocnemius under reducing
230 conditions to determine levels of irreversible ROS modification. Our results show that D2 *mdx*
231 mice but not C57 *mdx* mice have large amounts of cysteine adduction and tyrosine nitration (Figure
232 4G and H).

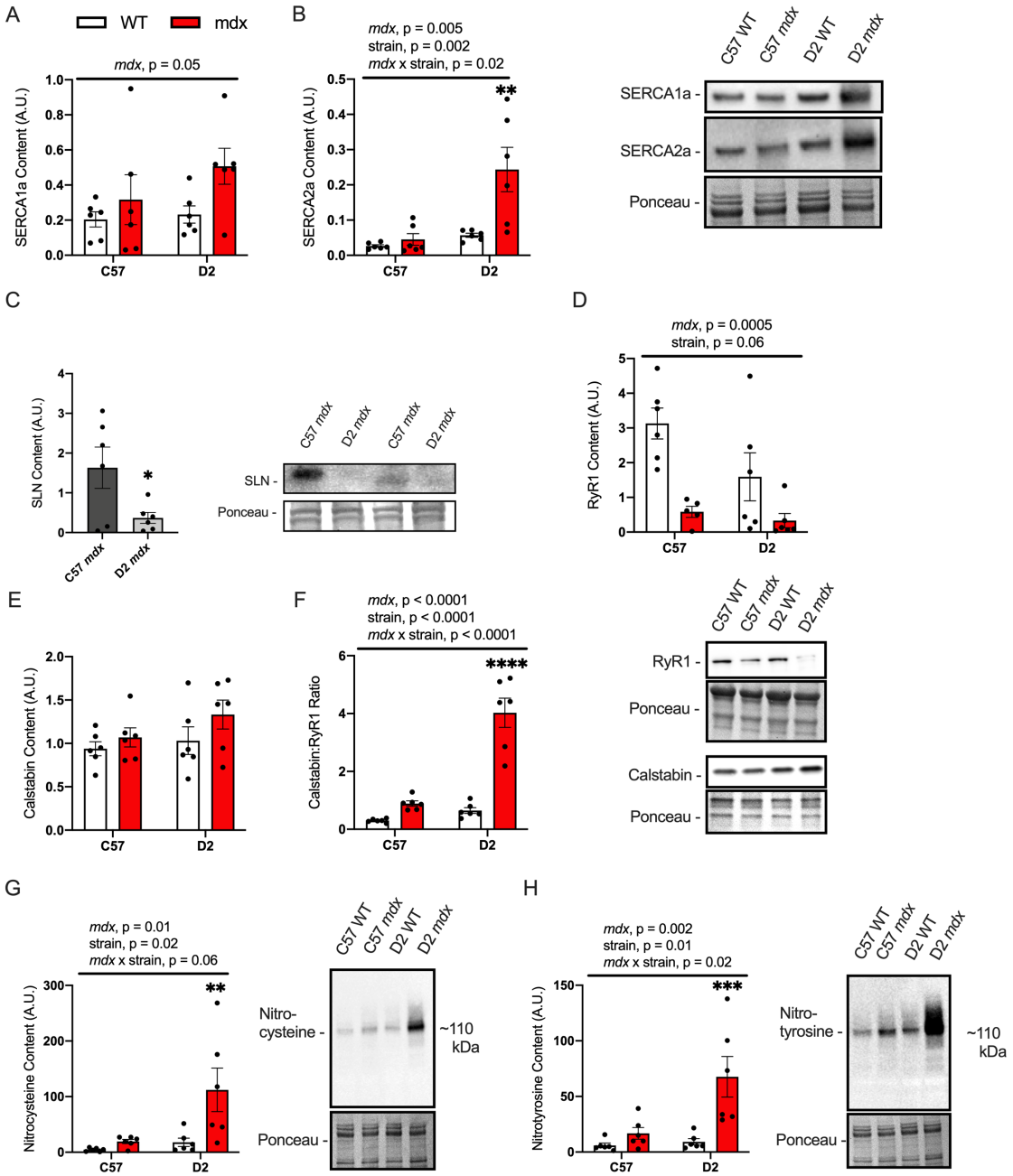

Figure 4: Western blot analyses of SR Ca^{2+} handling proteins total protein nitrosylation and tyrosine nitration: A) SERCA1a B) and SERCA2a content in gastrocnemius muscles from D2 and C57 -WT and -*mdx* mice. C) SLN content in gastrocnemius muscles from D2 *mdx* and C57 *mdx* mice. D) RyR1, E) calstabin, F) and calstabin:RyR1 content in gastrocnemius muscles from D2 and C57 -WT and -*mdx.* G) Protein nitrosylation measured via Western blotting for nitrocysteine-adducted protein. H) Protein tyrosine nitration measured via Western blotting for nitrotyrosine-adducted protein. For A,B and D-H, a two-way ANOVAs were performed with a Sidak's post-hoc test, $^{**}p < 0.01$, $^{***}p < 0.001$, $^{****}p < 0.0001$ n = 6 per group. Main effects and interactions expressed in bars over the graph. For C a Student's t-test was used, $^{*}p < 0.05$, n = 6 per group. All protein contents are expressed as arbitrary units. Values are represented as mean ± SEM.

244 *SR Ca^{2+} filling is also impaired in D2 mdx left ventricle and diaphragm muscles*

245 Given the cardiorespiratory implications of DMD, we also assessed SR Ca^{2+} handling in
246 cardiac (left ventricle) and diaphragm muscles from C57 and D2 -WT and -*mdx* mice. Similar to
247 our results with the gastrocnemius, we found that D2 *mdx* mice had severe decrements in Ca^{2+}
248 uptake in both the cardiac and diaphragm muscles (Figure 5). In the cardiac muscle, we found that
249 starting $[Ca^{2+}]_{free}$ was trending higher in the D2 *mdx* vs D2 WT, while this was not observed in the
250 C57 mice (Figure 5A and B). In addition, AUC was significantly higher in the D2 *mdx* vs D2 WT,
251 and this again was not observed in the C57 mice (Figure 5C). Though there were no differences,
252 apart from a main effect of strain on starting $[Ca^{2+}]_{free}$ in the diaphragm, a significant interaction
253 was again detected with AUC analysis, with only D2 *mdx* mice having significantly elevated AUC,
254 and thus impaired Ca^{2+} uptake vs D2 WT mice (Figure 5 D-F).

255

256

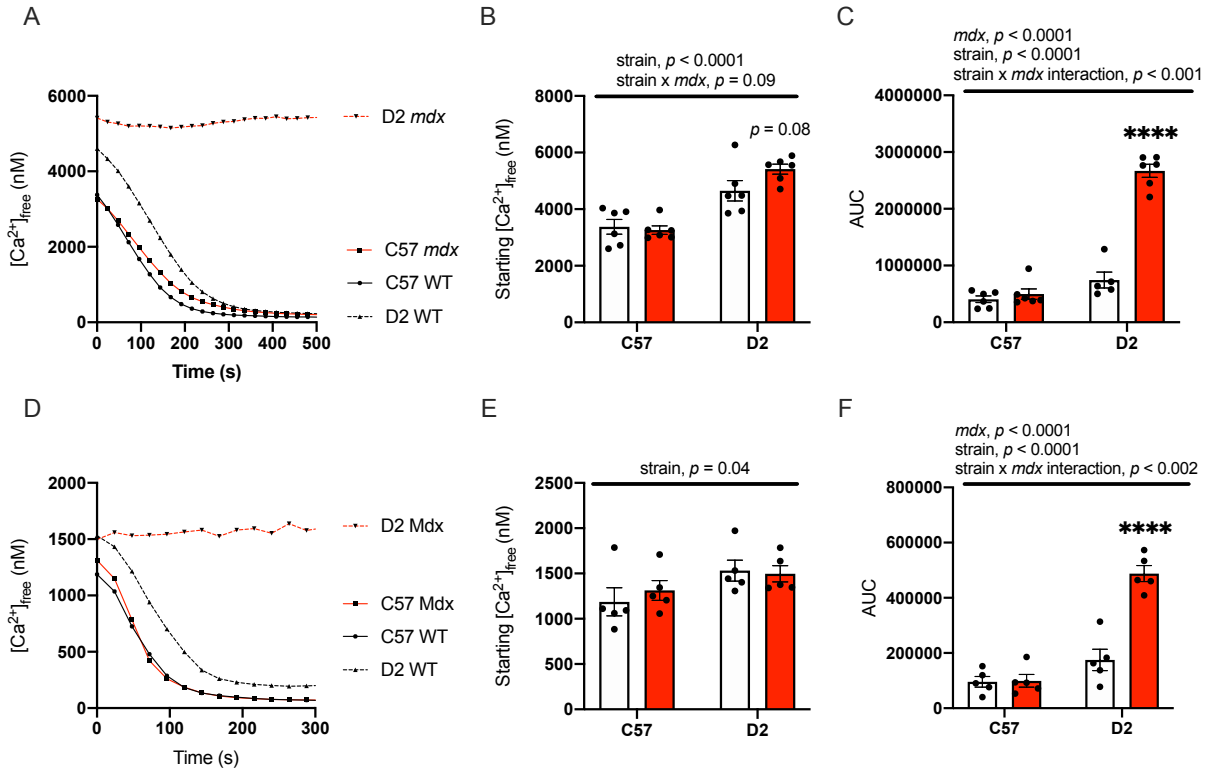

Figure 5: Ca^{2+} uptake in the cardiac and diaphragm muscles: A) Ca^{2+} uptake curves from left ventricle homogenates. B) Starting $[Ca^{2+}]_{free}$ levels immediately after ATP addition and C) AUC analysis in left ventricle homogenates. D) Ca^{2+} uptake curves from diaphragm homogenates. E) Starting $[Ca^{2+}]_{free}$ levels immediately after ATP addition and F) AUC analysis in diaphragm homogenates. Two-way ANOVAs were performed with a Sidak's post-hoc test, ****$p < 0.0001$, n= 5-6. Main effects and interactions expressed in bars over the graph. Values are represented as mean ± SEM.

273 **Discussion**

274 To our knowledge, this study is the first to compare SR Ca^{2+} handling in both the D2 *mdx*
275 mouse and C57 *mdx* mouse. The D2 *mdx* mouse is known as a more severe DMD model with early
276 onset weakness compared to the C57 *mdx* mouse. Impulse and measures of cage ambulation
277 supported that the D2 *mdx* mouse has more early on-set muscle weakness occurring at 8-10 weeks
278 of age. Also supporting this, the D2 *mdx* mouse had less interaction with the elevated mouse home
279 enclosure compared to C57 *mdx* mice. Interestingly, D2 *mdx* mice also had a hypermetabolic
280 profile, where these mice had the highest levels of energy expenditure while ambulating the least,
281 which we believe can contribute to the smaller body and muscle mass commonly observed in these
282 mice. Perhaps inconsistent with our results, Strakova et al. (2018) found that energy expenditure
283 was elevated in 5 month old C57 *mdx* mice compared with WT mice (23). We believe that this
284 discrepancy could possibly be explained by age differences, as our C57 *mdx* mice were younger
285 as compared to Strakova's mice.

286 To explain why the D2 *mdx* mice are much weaker at an earlier age, we explored the
287 involvement of SR Ca^{2+} handling and any potential disturbances. Our Ca^{2+} uptake and leak results
288 showed that D2 muscles (gastrocnemius, cardiac and diaphragm) had impaired ability to bring
289 Ca^{2+} into the SR. This manifested as an elevated starting $[Ca^{2+}]_{free}$, AUC during the uptake period
290 and lowered AUC throughout the leak period. In addition to these experiments, SERCA activity
291 in the gastrocnemius showed that Ca^{2+}-dependent ATP hydrolysis was impaired in D2 *mdx* but not
292 C57 *mdx* mice compared with their respective WT groups. Collectively, our findings with our Ca^{2+}
293 uptake assay and SERCA activity assay clearly showed that SR Ca^{2+} dysregulation is present in
294 young D2 *mdx* mice but not C57 *mdx* mice, which we believe ultimately contributes to the early-
295 onset weakness and sets these mice on a worsened trajectory for aging. Further, SR Ca^{2+}

296 dysregulation in the D2 *mdx* muscles may be a contributing factor to the elevated daily energy
297 expenditure seen in the metabolic caging data. Considering the large reductions in cage
298 ambulation, a high demand on Ca^{2+} regulation may contribute to the heightened energy
299 expenditure in the D2 *mdx* mice. Since intracellular Ca^{2+} is high in these mice, as indicated with a
300 higher starting $[Ca^{2+}]_{free}$ it is presumed that SERCA would be consuming a large amount of energy
301 to try and limit myoplasmic Ca^{2+} levels in the D2 *mdx* muscles. Further, this process may even
302 more inefficient due to limited SERCA function in these mice, creating a perpetual demand for
303 energy.

304 To explain the defective Ca^{2+} handling, we first examined SERCA protein levels. Both
305 SERCA1a and SERCA2a were upregulated in the gastrocnemius, which we believe is an adaptive
306 response aimed at improving SR Ca^{2+} handling. Indeed, SERCA density is an important
307 determinant of SR Ca^{2+} filling, at least in healthy conditions (24, 25). However, any compensatory
308 increase in SERCA content/density was unsuccessful in the rescuing SR Ca^{2+} handling in D2 *mdx*
309 mice. We next examined SLN expression. Although it is not typically expressed in murine
310 gastrocnemius muscle, ectopic expression of SLN occurred in both *mdx* mouse models, with SLN
311 protein being elevated to a greater extent in the C57 *mdx* mice compared to the D2 *mdx* mice.
312 Studies have shown that SLN is upregulated along with disease progression with its expression
313 being further upregulated in the *mdx*/utrophin double knockout mice compared with *mdx* mice
314 (14). Knocking out SLN in these mice improved dystrophic pathology suggesting that SLN may
315 contribute to *mdx* pathology. However, there are discrepant results with SLN deletion studies also
316 impairing *mdx* pathology or not changing the phenotype (26). Since we found that SLN was less
317 upregulated in the more severe D2 *mdx* mouse model with dramatic impairments in SERCA
318 function, our results could suggest that SLN may not be a critical player in the SERCA function

319 impairments and potentially *mdx* pathology in the D2 *mdx* mouse; however, this should be
320 investigated further specifically in the D2 *mdx* mouse. In addition, SLN is a known uncoupler of
321 SERCA and its upregulation in the D2 *mdx* mouse may contribute to the observed increase in daily
322 energy expenditure (27–29). However, even though SLN was more upregulated in C57 *mdx* mice,
323 these mice did not show elevated energy expenditure compared with C57 WT mice. Thus,
324 alternative mechanisms may be contributing to the increased energy expenditure. In this respect,
325 our results have shown dramatic impairments in Ca^{2+} uptake, and though SERCA activity was also
326 impaired, we were still able to measure viable rates of ATP hydrolysis. This disproportionate
327 impact on Ca^{2+} uptake vs ATP hydrolysis could be reflective of a highly inefficient system where
328 large amounts of ATP are required to regulate Ca^{2+} levels – thus contributing to the elevated energy
329 expenditure.

330 We then measured RyR1 and calstabin protein levels to further explore SR Ca^{2+} release
331 impairments. RyR1 content was reduced in D2 *mdx* mice, and calstabin:RyR1 content was
332 elevated. This may suggest that the gastrocnemius muscles reduced availability of RyR1 opening
333 to compensate for impairments in SR Ca^{2+} filling. This may also explain the reductions in SR Ca^{2+}
334 leak in our assay, however, this is difficult to determine as Ca^{2+} leak in our hands is very much
335 reliant on the level of SR Ca^{2+} filling. Therefore, while our assay determined that SERCA uptake
336 is impaired, it is still possible SR Ca^{2+} leak is enhanced, however, we cannot determine the nature
337 of the leak in these samples with our assays. Use of an assay that is less dependent on SR Ca^{2+}
338 filling should be used to better determine SR Ca^{2+} leak in D2 *mdx* mice.

339 Lastly, we measured total protein nitrosylation and tyrosine nitration in the gastrocnemius
340 to determine whether elevated RONS could contribute to the observed SR Ca^{2+} handling
341 dysfunction in the D2 *mdx* muscle. SERCA is susceptible to RONS damage and RONS are known

342 to be high in DMD, and therefore, it is plausible that RONS modifications could be contributing
343 to the changes in protein function we see (15, 30–34). Our results show that excessive and
344 irreversible (detection under reducing conditions) RONS modifications may be impairing function
345 of the SERCA pump. Moreover, damage to the SR membrane itself from RONS may contribute
346 to impairments in SR Ca^{2+} filling by leaking Ca^{2+} out during our uptake protocol altogether
347 contributing to the impairments in SR Ca^{2+} regulation.

348 We also determined the activation of calpain in D2 *mdx* gastrocnemius muscles. Calpain
349 is a Ca^{2+}-dependent proteolytic enzyme previously shown to be more active in *mdx* muscles (35).
350 To our knowledge, ours is the first study to demonstrate that rates of calpain activity are higher in
351 the D2 background compared to C57, irrespective of the *mdx* genotype. Furthermore, planned
352 comparisons between D2 *mdx* and C57 *mdx* reveals a significant 2.2-fold increase in calpain
353 activity in the former vs the latter ($p = 0.0006$ via Student's t-test). This finding is important and
354 adds mechanistic insight that may partly explain the worsened pathology in the D2 *mdx* mouse. It
355 is interesting that the D2 WT mice already had elevated calpain activation compared with C57
356 WT. This apparent difference in background strain may provide additional insight as to why *mdx*
357 mice on the D2 background are worse off than *mdx* mice on the C57 background. One explanation
358 that is not yet well understood, is a potential crosstalk between calpain activation and the pro-
359 fibrotic factor TGF-β. Previous studies have found that TGF-β1 upregulation in lung fibroblasts
360 and atrial derived myocytes can increase calpain activation (36, 37). This is interesting given recent
361 findings showing that a polymorphism of LTBP4 in D2 WT greatly upregulates TGF-β (38),
362 suggesting that the increased TGF-β activity could increase calpain activity in the D2 WT mice.
363 This combined with the impairments observed in SERCA function could contribute to elevated
364 calpain in the D2 *mdx* mice.

365 Though we did not specifically explore their contribution in our study, high intracellular
366 Ca^{2+} can lead to mitochondrial dysfunction in DMD pathology and may be an additional
367 contributing factor of Ca^{2+}-related pathology. Elevated myoplasmic Ca^{2+} can increase intake of
368 Ca^{2+} into the mitochondria which eventually leads to the opening of the mitochondrial
369 permeability transition pore (mPTP), then swelling and bursting of the mitochondria, excessive
370 H2O2 emission into the myoplasm, and subsequent calpain activation (39). A recent study by
371 Hughes and colleagues indeed found that D2 *mdx* mice have a greater number of swollen
372 mitochondria, increased susceptibility to mPTP opening in the quadriceps and excessive H2O2
373 emission (40). This could be contributing to the increased RONS released into the muscle and
374 subsequent SR Ca^{2+} handling dysfunction. Furthermore, the impairments in SR Ca^{2+} handling
375 could be perpetuating the mitochondrial dysfunction occurring in the D2 *mdx* mice, thereby
376 creating a vicious cycle leading to muscle degeneration and weakness.
377 In conclusion, our study clearly shows impairments in SR Ca^{2+} handling in skeletal and
378 cardiac muscles from D2 *mdx* mice, particularly at the level of the SERCA pump. Our results
379 suggest that the early onset weakness and damage observed in young D2 *mdx* mice may be partly
380 due to Ca^{2+} dysregulation. Future studies should investigate whether improving SERCA function,
381 potentially through cytotoxic protection against RONS may mitigate dystrophic pathology and
382 improve physiological outcomes in the D2 *mdx* mouse.
383
384
385
386
387

Methods

Animals and Design

Male C57 *mdx* (n = 12), C57 WT (n = 12), D2 *mdx* (n = 12), and D2 WT (n = 12) mice were purchased from Jackson Laboratories at 7-8 weeks of age. They were acclimated and housed in Brock University's Animal Facility, in an environmentally controlled room with a standard 12:12 hour light-dark cycle and allowed access to food and water *ad libitum*. After the mice reached 9-10 weeks of age, they were euthanized via cervical dislocation under general anesthetic (vaporized isoflurane) and their tissues were collected.

Hang Wire Testing

At 8-9 weeks of age, mice were subjected to a hang wire test to determine limb strength and endurance. All mice were gently placed on the wire situated 12 inches high and were left suspended on the wire until they reached exhaustion and dropped from the wire to the base of the cage. The time they remained suspended was recorded for three trials, separated by a 60s recovery period. Impulse (s*g) was calculated according to DMD_M.2.1.004 standard operating procedures by multiplying the average time suspended by body mass.

Metabolic Caging

At 8-9 weeks of age, mice were housed in pairs in a Promethion Metabolic Cage System for 48 hours. Two 12-hour light and dark cycles were measured, and data was collected. Food and water intake were measured through mass changes with the MM-1 load cell, the Promethion mass measurement device. Cage ambulation was quantified through metres travelled which is collected through beam breaks with the BXYZ Beambreak Activity Monitor in the x y, and z planes.

411 Respiratory exchange ratio (RER) was calculated as VCO_2 (volume of carbon dioxide expired each
412 minute) divided by VO_2 (volume of oxygen inspired each minute) measured from the Promethion
413 metabolic cages equipped with O_2 and CO_2 gas analyzers. To obtain mean energy expenditure
414 expressed in kcal/hr, the Weir equation was used (41).
415
416 *Sample Collection and Homogenization*
417 Gastrocnemius, diaphragm, and cardiac muscles (n=12/group) were rapidly extracted from
418 euthanized animals and flash frozen in liquid N2 and stored at -80˚C. For Ca^{2+} uptake and SERCA
419 activity analyses, muscles were homogenized in homogenizing buffer (5 mM HEPES, 250 mM
420 sucrose, 0.2 mM PMSF, 0.2% NaN3; pH 7.5). An aliquot of the muscle homogenate was then
421 supplemented with protease and phosphatase (phosSTOP; cOmplete Mini) inhibitors for western
422 blot analyses. Blood was collected via cardiac puncture and spun at 5000 x g for 8 minutes (4°C)
423 and serum was collected and stored at -80˚C.
424
425 *Serum Creatine Kinase Activity*
426 Serum creatine kinase activity was determined as previously described (42), with a M2
427 Molecular Device plate reader and a commercially available assay (Cat. #C7522, Pointe Scientific
428 Inc., Canton, MI, USA) fitted onto a 96-well plate and calibrated with a standard curve of purified
429 creatine kinase (Sigma, Oakville, ON, Canada, Cat. 10127566001).
430
431
432 *Sarcoplasmic Reticulum Ca^{2+} Uptake and Leak*

433 Ca^{2+} uptake assays were fitted onto a 96-well plate and done on a M2 Molecular Device
434 plate reader and the ratio-able Ca^{2+} fluorescent indicator Indo-1. In brief, 20 µl of diaphragm, 25
435 µl of gastrocnemius or 50 µl of left ventricle homogenate was added to 200 µl Ca^{2+} uptake buffer
436 (20mM HEPES, 200mM KCL, 10mM NaN_3, 5µM TPEN, 15mM $MgCl_2$, 5mM Oxalate; pH 7.0),
437 and 1 µl of Indo-1 (1 mM in 50 mM glycine, pH 7.0). Ca^{2+} uptake was initiated with 4 µl of ATP
438 (250 mM, pH 7.0) with the plate read kinetically set with an excitation wavelength of 355 nM and
439 emission wavelengths of 405 nm (Ca^{2+}-bound Indo-1) and 485 nm (Ca^{2+}-free Indo-1). After the
440 plateau was reached, 1 µl of cyclopiazonic acid (CPA) was added to inhibit the SERCA pump and
441 initiate SR Ca^{2+} leak. The plate was then read for an additional 600s. Free Ca^{2+} concentration was
442 calculated using the following formula and a Kd of 250 nM for Indo-1. The amount of Ca^{2+} uptake
443 and leak were measured through an area under the curve analysis (AUC). In addition, rates of Ca^{2+}
444 uptake and leak were analyzed and normalized to grams of protein measured by a BCA assay.
445

446 $$[Ca^{2+}] = K_d \left(\frac{R - R_{min}}{R_{max} - R}\right)\left(\frac{S_{f2}}{S_{b2}}\right)$$

447
448 Formula 1: Free Calcium Concentration ($[Ca^{2+}]_f$)
449 K_d is the dissociation constant of Indo-1 (250nM). R_{min} refers to the ratio of bound:unbound Indo-1 in the
450 EGTA portion. R_{max} refers to the ratio of bound:unbound Indo-1 in the high Ca^{2+} portion. S_{f2} is the
451 fluorescence emission at 485nm (Ca^{2+}-free Indo-1) in the EGTA portion and S_{b2} is the fluorescence
452 emission at 485nm in the high Ca^{2+} portion.
453

454 *SERCA ATPase Activity*

455 Ionophore (A23187; Sigma Aldrich) supported SERCA activity was measured in
456 gastrocnemius homogenates using an enzyme-linked spectrophotometric assay as previously
457 described (24, 30, 43). Briefly, muscle homogenates (15 µl), pyruvate kinase (PK) and lactate
458 dehydrogenase (LDH) (18 U I^{-1} for both) were added to Ca^{2+} ATPase buffer (20mM HEPES,

459 200mM KCl, 10mM NaN3, 1mM EGTA, 15mM MgCl2, 5mM ATP, 10mM
460 phosphoenolpyruvate). To initiate SERCA activity, 4 µl of 1.9% (w/v) NADH was added and the
461 plates were then read at 340 nm for 30 minutes. SERCA-dependent activity in gastrocnemius
462 homogenates was calculated with a pathlength correction, extinction coefficient of NADH (6.22
463 mM), and the subtraction of ATPase activity in the presence of 1 µl SERCA-specific inhibitor,
464 CPA (40 mM) from total ATPase activity across a range of Ca^{2+} concentrations (*p*Ca 6.95 – 5.75).
465 A bicinchoninic acid (BCA) assay was done to normalize SERCA activity to grams of protein.
466
467 *Western Blotting*
468 Western blotting was conducted to determine protein expression of SERCA1a/2a,
469 sarcolipin (SLN), RyR1 and calstabin. Laemmli buffer was added to muscle homogenates to
470 solubilize proteins that were then electrophorectially separated at 240V for 22 minutes on a 7-12%
471 TGX gradient gel (BioRad). Proteins were transferred to PVDF or nitrocellulose membranes for 6
472 minutes using BioRad Trans Blot Turbo. Prior to blocking, SuperSignal western Blot Enhancer
473 (46641) from Thermo Scientific was applied for the SLN blot. A 5% (w/v) milk and TBST solution
474 was used to block the membranes for one hour. Primary antibody was then added and incubated
475 overnight at 4°C. The primary antibodies SERCA1a (MA3-911), SERCA 2a (MA3-919), calstabin
476 (PA1-026A) were obtained from ThermoFisher Scientific (Waltham, MA, USA). The primary
477 antibody for SLN (ABT13) was obtained from Sigma-Aldrich (Oakville, ON, CA). The primary
478 antibody for nitrocysteine (ab94930) was obtained from Abcam (Cambridge, UK). The primary
479 antibody for nitrotyrosine (189542) was obtained from Cayman Chemical (Ann Arbor, MI, USA).
480 Subsequent to primary incubation, the membranes were washed three times with TBST and then
481 incubated with anti-mouse (SERCA1a/2a, RyR1 ;7076; Cell Signalling Technology) or anti-rabbit

482 (calstabin, SLN; 7074, Cell Signalling Technology,) secondary antibodies at room temperature for
483 1 hour. The membranes were then washed again three times with TBST then chemiluminescent
484 substrate Millipore Immobilon (WBKLS0500; Sigma-Aldrich) or SuperSignal West Femto
485 Maximum Sensitivity Substrate (34095; Thermo Scientific) was added prior to imaging with a
486 BioRad Chemidoc. Optical densities were analyzed with imageLab (BioRad) and normalized to
487 total protein visualized with a ponceau stain (59803; Cell Signalling Technology).
488
489 *Calpain Activity Assay*
490 A commercialized calpain assay (QIA120; Millipore Sigma) was used in order to
491 determine calpain activity in the gastrocnemius. Tissue was freshly homogenized in RIPA lysis
492 buffer and 50 μl of sample was loaded in duplicate in either 100 μl of activator buffer or 100 μl of
493 inhibitor buffer in a 96-well plate as per the manufacturer's instructions. Then, 50 μl of diluted
494 substrate was added in the dark into each well and the plate was incubated for 15 minutes. The
495 plate was then measured for 10 minutes as a kinetic plate at an excitation of 370 nm and emission
496 of 450 nm to determine the rate of calpain activity normalized to total protein (via BCA assay).
497
498 *Statistics*
499 A two-way ANOVA was used to test the main effects of genotype (*mdx*) and strain (C57
500 or D2) and their potential interaction for most analyses. Post-hoc testing was completed using
501 Sidak multiple comparison testing. A Student's t-test was also used to compare cage ambulation
502 data. Statistical tests were conducted using GraphPad Prism 8 Software (San Diego, USA). All
503 values are presented as means ± standard error. Statistical significance is set to $p \leq 0.05$.
504

Study Approval

All animal procedures were approved by the Brock University Animal Care and Utilization Committee (file #17-06-03) and were carried out in accordance with the Canadian Council on Animal Care guidelines.

Funding Sources

This work was supported by an unrestricted Brock University internal grant and a Canada Research Chair Tier 2 in Tissue Plasticity and Remodelling to VAF. REGC and SIH were supported by a NSERC CGS-M, and JLB was supported by a CIHR CGS-M.

516 **References**
517

518 1. Moat SJ, Bradley DM, Salmon R, Clarke A, Hartley, L. (2013) Newborn bloodspot screening
519 for Duchenne muscular dystrophy: 21 years experience in Wales (UK). *Eur. J. Hum. Genet.*
520 2013;21(10): 1049–1053. doi: 10.1038/ejhg.2012.301.
521
522 2. Emery AE. (1991) Population frequencies of inherited neuromuscular diseases - a world
523 survey. *Neuromuscul. Disord.* 1991;1(1):19–29. doi: 10.1016/0960-8966(91)90039-u.
524
525 3. Straub V, Balabanov P, Bushby K, et al. Stakeholder cooperation to overcome challenges in
526 orphan medicine development: the example of Duchenne muscular dystrophy. *Lancet*
527 *Neurol*. 2016;15(8):882–890. doi: 10.1016/S1474-4422(16)30035-7.
528
529 4. Emery AEH. The muscular dystrophies. *Lancet*. 2002;359(9307):687–695. doi:
530 10.1016/S0140-6736(02)07815-7.
531
532 5. Grigore I, Frasin M, Diaconu G. Cardiac complications in Duchenne muscular dystrophy in
533 children. *Rev Pediatr Obstet Ginecol Pediatr*. 2015;64(4):5. doi: 10.37897/RJP.2015.4.4.
534
535 6. Blake DJ, Weir A, Newey SE, Davies KE. Function and Genetics of Dystrophin and
536 Dystrophin-Related Proteins in Muscle. *Physiol Rev*. 2002;82(2):291–329. doi:
537 10.1152/physrev.00028.2001.
538
539 7. Tubridy N, Fontaine B, Eymard B. Congenital myopathies and congenital muscular
540 dystrophies. *Curr. Opin. Neurol.* 2001;14(5):575–582. doi: 10.1097/00019052-200110000-
541 00005.
542
543 8. Shin J, Tajrishi MM, Ogura Y, Kumar A. Wasting mechanisms in muscular dystrophy. *Int J*
544 *Biochem Cell Biol*. 2013;45(10):2266–2279. doi: 10.1016/j.biocel.2013.05.001.
545
546 9. Santulli G, Lewis D, des Georges A, Marks AR, Frank J. Ryanodine Receptor Structure and
547 Function in Health and Disease. *Subcell. Biochem.* 2018;87:329–352. doi: 10.1007/978-981-
548 10-7757-9_11.
549
550 10. MacLennan DH, Rice WJ, Green NM. The Mechanism of Ca^{2+} Transport by
551 Sarco(Endo)plasmic Reticulum Ca^{2+}-ATPases. *J. Biol. Chem.* 1997;272(46):28815–28818.
552 doi: 10.1074/jbc.272.46.28815.
553
554 11. Turner PR, Westwood T, Regen CM, Steinhardt RA. Increased protein degradation results
555 from elevated free calcium levels found in muscle from mdx mice. *Nature*. 1988;335
556 (6192):735–738. doi: 10.1038/335735a0.
557
558 12. Robert V, Massimino ML, Tosello V, Marsault, et al. Alteration in calcium handling at the
559 subcellular level in mdx myotubes. *J. Biol. Chem.* 2001;276(7):4647–4651. doi:
560 10.1074/jbc.M006337200.
561

13. Bellinger AM, Reiken S, Carlson C, et al. Hypernitrosylated ryanodine receptor/calcium release channels are leaky in dystrophic muscle. *Nat Med*. 2009;15(3):325–330. doi: 10.1038/nm.1916.

14. Voit A, Patel V, Pachon R, et al. Reducing sarcolipin expression mitigates Duchenne muscular dystrophy and associated cardiomyopathy in mice. *Nat Commun*. 2017;8(1). doi: 10.1038/s41467-017-01146-7.

15. Gehrig SM, van der Poel C, Sayer TA, et al. Hsp72 preserves muscle function and slows progression of severe muscular dystrophy. *Nature*. 2012;484(7394):394–398. doi: 10.1038/nature10980.

16. Bulfield G, Siller WG, Wight PA, Moore KJ. X chromosome-linked muscular dystrophy (mdx) in the mouse. *Proc Natl Acad Sci U S A*. 1984;81(4):1189–1192. doi: 10.1073/pnas.81.4.1189.

17. Swiderski K, Lynch GS. Murine models of Duchenne muscular dystrophy: is there a best model? *Am J Physiol Cell Physiol*. 2021;321(2) doi: 10.1152/ajpcell.00212.2021.

18. Coley WD, Bogdanik L, Vila MC. et al. Effect of genetic background on the dystrophic phenotype in mdx mice. *Hum. Mol. Genet.* 2016;25(1):130–145. doi: 10.1093/hmg/ddv460.

19. Hammers DW, Hart CC, Matheny MK, et al. The D2.mdx mouse as a preclinical model of the skeletal muscle pathology associated with Duchenne muscular dystrophy. *Sci Rep*. 2020;10(1):14070. doi: 10.1038/s41598-020-70987-y.

20. van Putten M, Putker K, Overzier M, et al. Natural disease history of the D2-mdx mouse model for Duchenne muscular dystrophy. *FASEB J*. 2019;33(7):8110–8124. doi: 10.1096/fj.201802488R.

21. Mázala DAG, Novak JS, Hogarth MW, et al. (2020) TGF-β–driven muscle degeneration and failed regeneration underlie disease onset in a DMD mouse model. *JCI Insight*. 2020;5(6):e135703. doi: 10.1172/jci.insight.135703.

22. Schneider JS, Shanmugam M, Gonzalez JP, et al. Increased sarcolipin expression and decreased sarco(endo)plasmic reticulum Ca2+ uptake in skeletal muscles of mouse models of Duchenne muscular dystrophy. *J. Muscle Res. Cell. Motil.* 2013;34(5-6):349–356. doi: 10.1007/s10974-013-9350-0.

23. Strakova J, Kamdar F, Kulhanek D, et al. Integrative effects of dystrophin loss on metabolic function of the mdx mouse. *Sci Rep*. 2018;8(1):13624. doi: 10.1038/s41598-018-31753-3.

24. Hamstra SI, Kurgan N, Baranowski RW, et al. Low-dose lithium feeding increases the SERCA2a-to-phospholamban ratio, improving SERCA function in murine left ventricles. *Exp Physiol*. 2020;105(4):666–675. doi: 10.1113/EP088061.

25. Smith IC, Bombardier E, Vigna C, Tupling AR. ATP Consumption by Sarcoplasmic Reticulum Ca2+ Pumps Accounts for 40-50% of Resting Metabolic Rate in Mouse Fast and Slow Twitch Skeletal Muscle. *PLoS ONE*. 2013;8(7):e68924. doi: 10.1371/journal.pone.0068924.

26. Bal NC, Gupta SC, Pant M, et al. Is Upregulation of Sarcolipin Beneficial or Detrimental to Muscle Function? *Front Physiol*. 2021;12:633058. doi: 10.3389/fphys.2021.633058.

27. Smith WS, Broadbridge R, East JM, Lee AG. Sarcolipin uncouples hydrolysis of ATP from accumulation of Ca2+ by the Ca2+-ATPase of skeletal-muscle sarcoplasmic reticulum. *Biochem J*. 2002;361(2):277–286. doi: 10.1042/0264-6021:3610277.

28. Bombardier E, Smith IC, Vigna C, Fajardo VA, Tupling AR. Ablation of sarcolipin decreases the energy requirements for Ca2+ transport by sarco(endo)plasmic reticulum Ca2+-ATPases in resting skeletal muscle. *FEBS Lett*. 2013;587(11):1687–1692. doi: 10.1016/j.febslet.2013.04.019.

29. Mall S, Broadbridge R, Harrison SL, et al. The presence of sarcolipin results in increased heat production by Ca(2+)-ATPase. *J Biol Chem*. 2006;281(48):36597–36602. doi: 10.1074/jbc.M606869200.

30. Braun JL, Hamstra SI, Messner HN, Fajardo VA. SERCA2a tyrosine nitration coincides with impairments in maximal SERCA activity in left ventricles from tafazzin-deficient mice. *Physiol Rep*. 2019;7(16):e14215. doi: 10.14814/phy2.14215.

31. Fu M, Bombardier E, Gamu D, Tupling AR. Phospholamban and sarcolipin prevent thermal inactivation of sarco(endo)plasmic reticulum Ca2+-ATPases. *Biochem J*. 2020;477(21):4281–4294. doi: 10.1042/BCJ20200346.

32. Fajardo VA, Trojanowski N, Castelli LM, et al. Saturation of SERCA's lipid annulus may protect against its thermal inactivation. *Biochem Biophys Res Commun*. 2017;484(2):456–460. doi: 10.1016/j.bbrc.2017.01.154.

33. Fu MH, Tupling AR. Protective effects of Hsp70 on the structure and function of SERCA2a expressed in HEK-293 cells during heat stress. *Am. J. Physiol. Heart Circ. Physiol.* 2009;296(4):H1175-1183. doi: 10.1152/ajpheart.01276.2008.

34. Tupling AR. Protection of heart and skeletal muscle by heat shock proteins. *Appl Physiol Nutr Metab*. 2008;33(5):1021–1022. doi: 10.1139/H08-066.

35. Gailly P, De Backer F, Van Schoor M, Gillis JM. In situ measurements of calpain activity in isolated muscle fibres from normal and dystrophin-lacking mdx mice. *J Physiol*. 2007;582(3):1261–1275. doi: 10.1113/jphysiol.2007.132191.

652 36. Li F-Z, Cai P-C, Song L-J, et al. Crosstalk between calpain activation and TGF-β1 augments
653 collagen-I synthesis in pulmonary fibrosis. *Biochim Biophys Acta Mol Basis Dis*.
654 2015;1852(9):1796–1804. doi: 10.1016/j.bbadis.2015.06.008.
655
656 37. Yeh Y-H, Kuo C-T, Chan T-H, et al. Transforming growth factor-β and oxidative stress
657 mediate tachycardia-induced cellular remodelling in cultured atrial-derived myocytes.
658 *Cardiovasc Res*. 2011;91(1):62–70. doi: 10.1093/cvr/cvr041.
659
660 38. Heydemann A, Ceco E, Lim JE, et al. Latent TGF-β–binding protein 4 modifies muscular
661 dystrophy in mice. *J. Clin. Invest.* 2009;119(12):3703–3712. doi: 10.1172/JCI39845.
662
663 39. Timpani CA, Hayes A, Rybalka E. Revisiting the dystrophin-ATP connection: How half a
664 century of research still implicates mitochondrial dysfunction in Duchenne Muscular
665 Dystrophy aetiology. *Med Hypotheses*. 2015;85:1021–1033.
666
667 40. Hughes MC, Ramos SV, Turnbull PC, et al. Early myopathy in Duchenne muscular
668 dystrophy is associated with elevated mitochondrial H2 O2 emission during impaired
669 oxidative phosphorylation. *J Cachexia Sarcopenia Muscle*. 2019;10(6):643–661. doi:
670 10.1016/j.mehy.2015.08.015.
671
672 41. Weir JB de V. New methods for calculating metabolic rate with special reference to protein
673 metabolism. *J Physiol*. 1949;109(1-2):1–9. doi: 10.1113/jphysiol.1949.sp004363.
674
675 42. McKinlay BJ, Theocharidis A, Adebero T, et al. Effects of Post-Exercise Whey Protein
676 Consumption on Recovery Indices in Adolescent Swimmers. *IJERPH*. 2020(21);17:7761.
677 doi: 10.3390/ijerph17217761.
678
679 43. Hamstra SI, Whitley KC, Baranowski RW, et al. The role of phospholamban and GSK3 in
680 regulating rodent cardiac SERCA function. *Am. J. Physiol., Cell Physiol.* 2020;319(4). doi:
681 10.1152/ajpcell.00318.2020.